Biophysical Chemistry 190–191 (2014) 17–24

Contents lists available at ScienceDirect

Biophysical Chemistry

journal homepage: http://www.elsevier.com/locate/biophyschem

Interaction of Metallo- and free base *meso*-tetrakis(*N*-methylpyridium-4-yl)porphyrin with a G-quadruplex: Effect of the central metal ions

Yun-Hwa Kim [a], Changyun Lee [a], Seog K. Kim [a,*], Sae Chae Jeoung [b,*]

[a] Department of Chemistry, Yeungnam University, 214 Dae-dong, Gyeongsan City, Gyeong-buk 712-749, Republic of Korea
[b] Center for Medical Measurements, Korea Research Institute of Standards and Science, 267 Gajeong-Ro, Yuseong-Gu, Daejeon 305-340, Republic of Korea

HIGHLIGHTS

- The interaction of metallo- and non-metallo-porphyrins and $5'G_2T_2G_2TGTG_2T_2G_2$ G-quadruplex was investigated.
- None of the tested porphyrins intercalates to G-quadruplex.
- Both ZnTMPyP and VOTMPyP were able to stabilize the G-quadruplex with higher efficiency for ZnTMPyP.

GRAPHICAL ABSTRACT

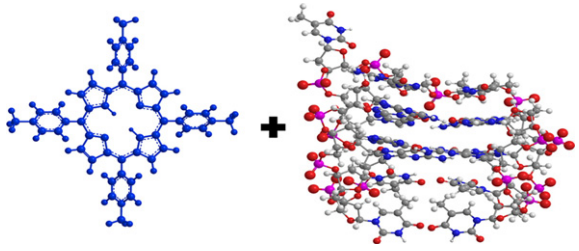

ARTICLE INFO

Article history:
Received 26 January 2014
Received in revised form 18 March 2014
Accepted 21 March 2014
Available online 1 April 2014

Keywords:
DNA
G-quadruplex
Porphyrin
Circular dichroism
Fluorescence

ABSTRACT

The effects of the central metal ion on complex formation between *meso*-tetrakis(*N*-methylpyridium-4-yl)porphyrin (TMPyP) and the thrombin-binding aptamer G-quadruplex, $5'G_2T_2G_2TGTG_2T_2G_2$, were examined in this study. The central metal ions were vanadium and zinc. At a [porphyrin]/[G-quadruplex] ratio of less than one, the absorption and CD spectra were unaffected by the mixing ratio for all three porphyrins, suggesting that the binding mode is homogeneous. Relatively small changes in the absorption spectrum when forming the complexes with the G-quadruplex, the positive CD signal, and the large accessibility of the I^- quencher, suggested that all these porphyrins are not intercalated between the G-quartet. Stabilization of the G-quadruplex by ZnTMPyP was most effective. The effect of VOTMPyP on G-quadruplex stabilization was moderate, whereas TMPyP slightly destabilized G-quadruplex. From this observation, the involvement of the ligation of one G-quartet component to the central metal ion in G-quadruplex stabilization by metallo-TMPyP is suggested

1. Introduction

The structure and dynamics of G-quadruplexes with a G-quartet structure composed of four G-bases connected via Hoogsteen type hydrogen bonding in the same plane have received considerable attention because of their biological importance [1–5]. The G-quadruplex can influence a number of biological processes, such as gene rearrangement, promoter activation, and blocks the binding of telomerase [6]. Designing molecules including a number of metal complexes that can identify and bind selectively to these sequences has attracted considerable attention because of their potential biological applications in the development of anticancer drugs [7]. Such metal complexes include porphyrin derivatives, metal salphen complexes [8,9], metal terpyridine complexes [10,11] and Ru(II) complexes with planar aromatic polycyclic rings [12–15]. Among these molecules, free base and metallo cationic porphyrin derivatives are the earliest examples that bind to the telomeric G-quadruplexes. As an example, certain Mn(III)porphyrin derivatives showed 10,000-fold selectivity for the G-quadruplex with a human terometric $5'AG_3TTAG_3TTAG_3TTAG_3$ sequence over duplex DNA [16]. The biological importance of the interaction of cationic porphyrin and G-quadruplex was highlighted by the discovery that certain porphyrin derivatives inhibit telomerase activity in HeLa cells [17–19].

* Corresponding authors. Tel.: +82 53 810 2362; fax: +82 53 815 5412.
E-mail addresses: seogkim@yu.ac.kr (S.K. Kim), scjeung@kriss.re.kr (S.C. Jeoung).

http://dx.doi.org/10.1016/j.bpc.2014.03.005
0301-4622/

Understanding the binding mode and interaction of porphyrin derivatives to G-quadruplexes is important for the rational application of these promising cationic molecules. Various binding modes of free base and metallo-porphyrin to G-quadruplex have been reported including the intercalation of planar porphyrin between two adjacent G-quartets [20–26], stacking on the external G-tetrads [18,19,21,27–34] and weak external binding [16,21,35–38] via electrostatic interaction. Many factors, such as the nature of the G-quadruplex, nature of the central metal ion, structure of the periphery groups, and solution condition, appear to affect the binding mode. For example, two contrasting binding modes for typical cationic porphyrin, *meso*-tetrakis(1-methylpyridinium-4-yl)porphyrin (referred to as TMPyP), have been reported. Molecular dynamic and isothermal titration calorimetric study have suggested an intercalative binding mode for TMPyP at each close GpG site of $AG_3(T_2AG_3)_3$, $[d(T_4G_4)]_4$ and $d(G_2T_2G_2TGTG_2T_2G_2)$ quadruplex. On the other hand, TMPyP was reported to bind to the parallel and antiparallel hybrids of the $AG_3(T_2AG_3)_3$ G-quadruplex by end-stacking and an external groove binding mode [21,28]. A heterogeneous binding mode at a high [porphyrin]/[G-quadruplex] ratio (referred to as T ratio) was also reported: one of the TMPyP intercalates between G-quartet whereas another TMPyP binds at the groove of the parallel $AG_3(T_2AG_3)_3$ G-quadruplex in the presence of poly(ethylene glycol). The nature of the central metal ion and the size of G-quartet also appear to affect the binding mode. Planar CuTMPyP stacks both ends of the parallel $(T_4G_4T_4)_4$ quadruplex, whereas it intercalates between G-quartet in addition to end-stacking on the $(T_4G_8T_4)_4$ quadruplex [32,33], suggesting that the length of the G-quartet may be one of the essential factors in determining the binding mode of planar porphyrin. When the central metal possesses an axial ligand such as ZnTMPyP, porphyrins bind to $[d(TAGGG)_2]_2$ and $AG_3(T_2AG_3)_3$ quadruplex by end-stacking [27,29].

In the duplex DNA case, the presence of the axial ligand is one of the essential factors governing the binding mode of porphyrin [39,40]. At a low R ratio, planar porphyrins namely free base TMPyP, CuTMPyP and NiTMPyP intercalate between the DNA base pairs, whereas those with the axial ligand, VOTMPyP, TiOTMPyP, CoTMPyP and MnTMPyP, exhibited external binding mode with a ~60° tilt in their electric transition moments with respect to the local DNA helix axis. With increasing porphyrin concentration, they begin to stack, disregarding the distinctive binding mode at low R ratios. In this study, the effect of the central metal ions, i.e., VO and Zn, on the binding mode of porphyrins to a G-quadruplex, thrombin-binding aptamer $5'G_2T_2G_2TGTG_2T_2G_2$, was investigated using a range of fluorescence techniques, absorption and circular dichroism (CD) spectra. A NMR study revealed the structure of the aptamer $5'G_2T_2G_2TGTG_2T_2G_2$ to be "antiparallel" [41].

2. Materials and methods

2.1. Materials

TMPyP and MTMPyP (M = Cu, VO and Zn, Fig. 1) were purchased from Frontier Scientific Inc. (Logan, Utah) and the thrombin-binding aptamer $5'G_2T_2G_2TGTG_2T_2G_2$ (Fig. 1) was purchased from SBS Genetech Co., Ltd. (China). These materials were dissolved in a pH 7.0 5 mM cacodylate buffer and used as received. The concentrations of porphyrins and oligonucleotide were determined by spectrophotometry using the following molar extinction coefficients: $\varepsilon_{421\ nm} = 2.45 \times 10^5\ M^{-1}\ cm^{-1}$, $\varepsilon_{438\ nm} = 2.07 \times 10^5\ M^{-1}\ cm^{-1}$, $\varepsilon_{436\ nm} = 2.04 \times 10^5\ M^{-1}\ cm^{-1}$ and $\varepsilon_{260\ nm} = 1.43 \times 10^5\ M^{-1}\ cm^{-1}$ for TMPyP, VOTMPyP, ZnTMPyP and the oligonucleotide, respectively. The quadruplex was formed by addition of 100 mM KCl followed by heating at 80 °C for 10 min and annealing overnight at room temperature. The formation of the quadruplex was confirmed by its characteristic CD spectrum. Aliquots of a concentrated TMPyP solution were added to a 5 μM polynucleotide solution (typically few μL to 3 mL polynucleotide solution) for the absorption and CD measurements, and appropriate corrections were made for the volume change. The mixing ratio, R, is defined by the ratio of the molar concentration of porphyrin to the G-quadruplex forming aptamer, i.e., [porphyrin]/[Q-quadruplex]. The samples were diluted 10 fold for fluorescence measurement to avoid the inner filter effect.

2.2. Measurement

The CD spectra were obtained using either a Jasco J-715 or a J-810 spectropolarimeter (Tokyo, Japan). The absorption and steady state fluorescence spectra were recorded using a Cary 100 spectrophotometer (Palo Alto, CA) and Sinco FS-2 (Seoul, Korea). The fluorescence decay profiles for porphyrins bound to the quadruplex were measured using the time-correlated single photon counting method [42]. The pulsed excitation laser was obtained by second harmonic generation of fundamental output from the combination of linear parametric amplifier (Orpheus, Lithuania) and generative amplified femtosecond laser (Pharos, Lithuania). The resultant output has a pulse width less than 300 fs, bandwidth less than 10 nm and pulse repetition rate of 200 kHz. The photoluminescence was dispersed by a spectrometer (Model HR320, Jovin Yvon, France) and the resultant emission was detected by an avalanche photodiode and fed into a time-correlated single photon counting module (TCSPC) (Model SPC-130, Becker & Hickl, Germany). The full-width at half maximum of instrumental response function was 0.12 ns. The emission wavelength was 657 nm for TMPyP and VOTMPyP and was 630 nm for ZnTMPyP. The illumination power was kept low enough to observe no apparent emission intensity changes before and after measurement.

The fluorescence quenching experiment was carried out by the addition of NaI at various concentrations. The concentration of the counter ion, Na^+, can influence the result by affecting the conformation of quadruplex and/or the extent of porphyrin-quadruplex complex formation. Therefore, $[Na^+]$ was kept constant throughout the quenching experiment by adding the appropriate concentration of NaCl. The accessibility of the I^- quencher can be obtained from the well-known Stern–Volmer plot [43].

$$\frac{F_0}{F} = 1 + K_{SV}[Q] \tag{1}$$

where F_0 and F denote the fluorescence intensity in the absence and presence of a quencher, respectively, and K_{SV} is the Stern–Volmer quenching constant that reflects the extent of the accessibility of the quencher to the fluorophore. In the static quenching case, in which the fluorescence is quenched by the formation of a non-fluorescent complex between the fluorophore and quencher, K_{SV} is considered to be the equilibrium constant for complex formation. In the dynamic quenching mechanism, in which the fluorophore loses its excited energy by collisions with the quencher, K_{SV} is related to the collision frequency.

The concept of "contact energy transfer" was first reported for energy transfer from the DNA base to intercalated ethidium [44]. When the ratio of the quantum yield of intercalated ethidium to that of DNA-free porphyrins was plotted with respect to the wavelength in the DNA absorption region, the shape of the plot was similar to the DNA absorption spectrum, indicating that the energy is transferred from excited DNA bases to intercalated ethidium. The amount of energy transfer, i.e. the ratio of the quantum yield, was calculated for each wavelength using the expression,

$$Q(\lambda) = \frac{I_b(\lambda)\varepsilon_f(\lambda)}{I_f(\lambda)\varepsilon_b(\lambda)} \tag{2}$$

where I and ε are the measured fluorescence intensity and absorbance at wavelength, λ, respectively, and b and f denote the bound and free

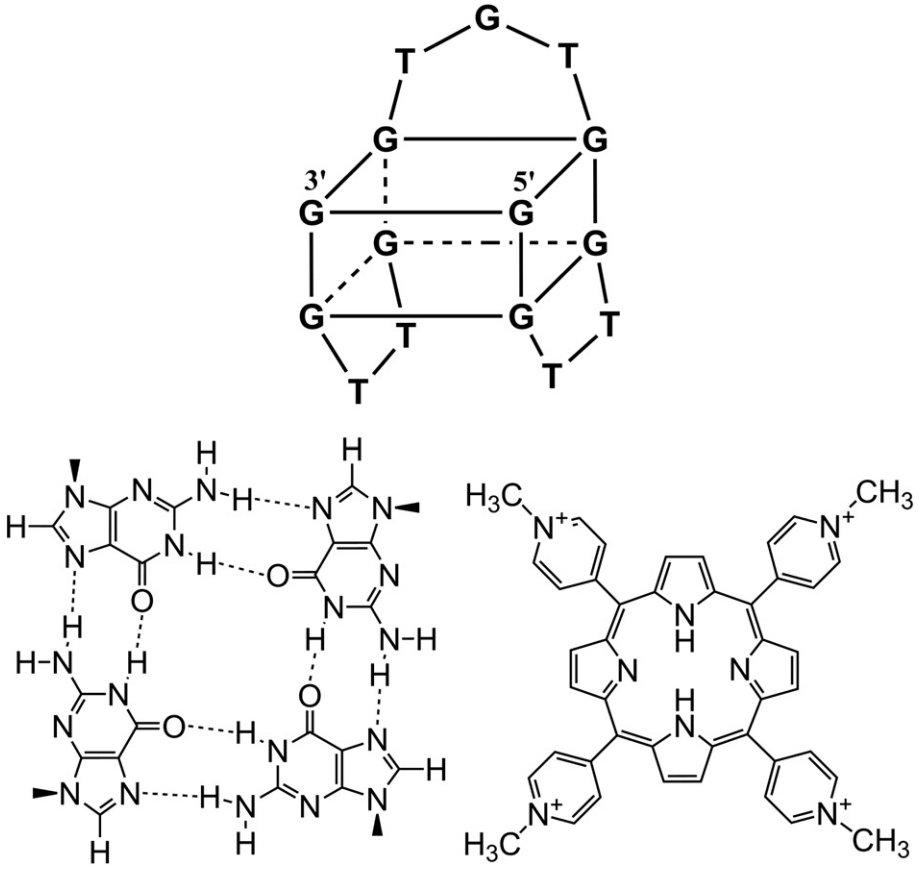

Fig. 1. Schematic diagram of the G-quadruplex and the chemical structure of TMPyP.

ligands, respectively. The ratio $Q(\lambda)/Q_{320\ nm}$ was plotted with respect to the wavelength. The normalization factor, $Q_{320\ nm}$, was chosen because DNA does not absorb at this wavelength. Although this concept has been used occasionally as an indication of ligand intercalation, minor groove binding ligands were found to produce similar energy transfer [45]. Therefore, this concept was used to show that the porphyrin and G-quartet of the quadruplex is in close contact.

3. Result

3.1. Absorption and CD spectra

In the duplex DNA case, intercalators produce a large red shift and hypochromism in the absorption region of the ligand due to a change in the environmental polarity and the π–π interaction between the DNA bases and the intercalated ligand. On the other hand, the change in the absorption spectrum of the minor groove binding ligand is normally the result of a change in the molecular conformation of the ligand in addition to the change in the environmental polarity and strong transition moment dipole coupling between the base pairs and the ligand. Fig. 2 compares the absorption spectra of various cationic porphyrins bound to the G-quadruplex. The shape of the absorption spectrum was constant at R = 0.2, 0.4, 0.6, 0.8, and 1.0. Therefore, only those for R = 1.0 are presented for clarity. Upon binding to the Q-quadruplex, metal-free TMPyP produced a 5 nm red shift (from 422 nm to 427 nm) and ~25% hypochromism in the Soret absorption region (Fig. 2, panel A). Although the system is completely different, the absorption spectrum of TMPyP intercalated to double stranded native DNA is shown for comparison. When TMPyP was fully intercalated between the base pairs of double stranded DNA, it produced a ~20 nm red shift and 47% hypochromism which are in accordance with previous reports [39,40]. ZnTMPyP exhibited a 5 nm red shift and ~11% hypochromism (Fig. 2, panel C). In the VOTMPyP case, small hypochromism of ~11% without a shift in the absorption maximum was observed in the presence of the G-quadruplex (Fig. 2, panel C).

Although porphyrins are achiral, they produce a CD signal upon binding to double stranded DNAs. The origin of this induced CD in the Soret region is believed to be the interaction of the B_x and B_y electric transition moments of porphyrin with those of chirally-arranged DNA bases. In the double stranded DNA case, a negative CD band in the Soret band was considered to be a diagnostic of the intercalation of porphyrin between the DNA base pairs, whereas a positive band may reflect the external binding mode [40]. Fig. 3 shows the CD spectrum of TMPyP, VOTMPyP and ZnTMPyP bound to the G-quadruplex at R = 1.0. In addition to the absorption spectra, the CD spectrum recorded for the other R ratios, 0.2, 0.4, 0.6, 0.8, and 1.0, were identical for all porphyrins. Therefore, only an R ratio of 1.0 is shown for simplicity. All porphyrins showed a positive CD band in the Soret absorption region centered at ~430 nm, ~435 nm and ~446 nm for TMPyP, VOTMPyP and ZnTMPyP, respectively. In the VOTMPyP case, a small second positive CD band was also visible at a longer wavelength (~458 nm). Although it is not clear, differences in the interactions with DNA bases with the two electric transitions of VOTMPyP may cause the appearance of the two CD band in the Soret region. The similar positive shape of the CD spectra of TMPyP to those with axial ligands suggests that despite its planar shape, TMPyP does not intercalate to G-quadruplex. A bisignate CD spectrum was reported in the Soret absorption region for the ZnTMPyP complexed with the Pb^{2+} induced $AG_3(T_2AG_3)_3$ G-quadruplex [29], which is in contrast to the current result. This discrepancy can be attributed to the difference in the number of G-quartets and the nature of the stabilizing cation.

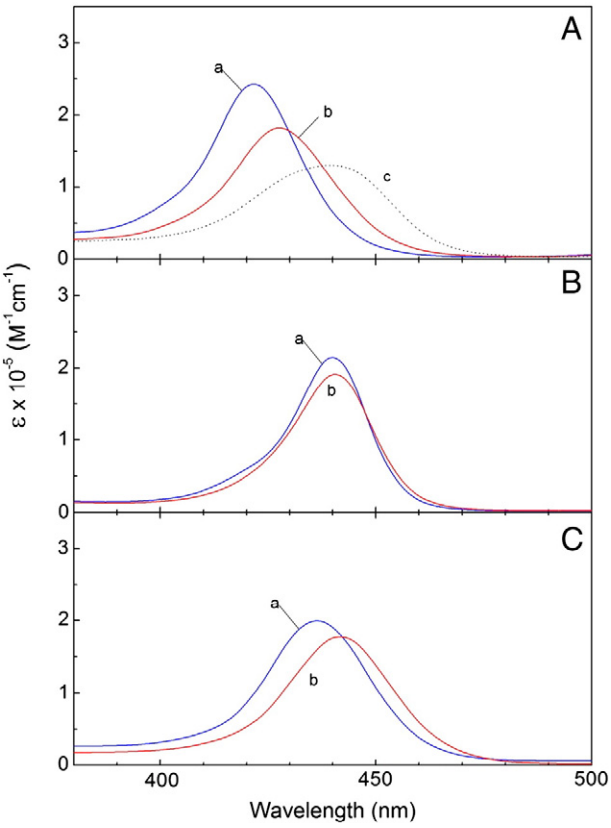

Fig. 2. Absorption spectrum of TMPyP (panel (A)), VOTMPyP (panel (B)) and ZnTMPyP (panel (C)) bound to the G-quadruplex at R ratio of 0.2, 0.4, 0.6, 0.8 and 1.0. The absorption spectra were identical hence, only the data at R = 1.0 is shown (curve b) for clarity. G-quadruplex-free porphyrins (curves a) are compared in each case. In panel (A), absorption spectrum of DNA-intercalated TMPyP (curve c) is also compared. [G-quadruplex] = 5 μM and [KCl] = 100 mM. Curve c in panel (A) was recorded for the 2.5 μM TMPyP in the presence of 100 μM native calf thymus DNA.

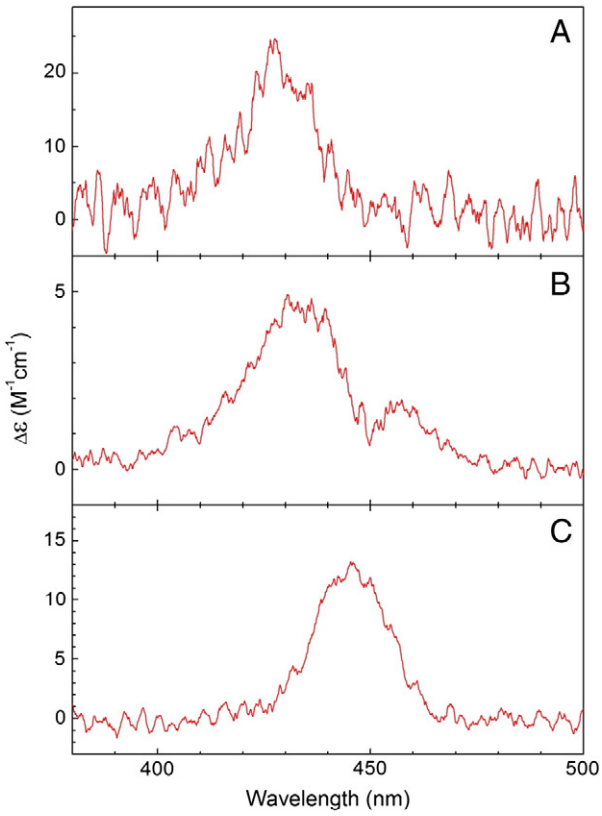

Fig. 3. CD spectrum of TMPyP (panel (A)), VOTMPyP (panel (B)) and ZnTMPyP (panel (C)) bound to G-quadruplex at the R ratio of 1.0. The CD spectra recorded for other mixing ratio at R = 0.2, 0.4, 0.6, 0.8 were identical. The CD signals were averaged over 5 scans. [G-quadruplex] = 5 μM and [KCl] = 100 mM.

Fig. 4 shows the effects of various porphyrins on the thermal stability of the G-quadruplex. The aptamer 5′$G_2T_2G_2TGTG_2T_2G_2$ exhibited a characteristic CD spectrum in the DNA absorption region with its positive maxima at 293 nm and 248 nm, and a negative minimum at 266 nm in the presence of 100 mM KCl at 20 °C (Fig. 4b, insertion), suggesting the formation of an antiparallel type G-quadruplex. At high temperatures (80 °C), the CD spectrum disappeared: a transition from the G-quadruplex to a single stranded oligonucleotide occurred. In the absence of porphyrin, the temperature at which a 50% transition occurred was ~51.5 °C. The presence of TMPyP reduced the transition temperature slightly: 50.5 °C at R = 0.5 and was 49.0 °C at R = 1.0. A further increase in the TMPyP concentration did not affect the transition temperature. The binding of VOTMPyP increased the transition temperature slightly: 53.0 °C and 54.0 °C at R ratios of 0.5 and 1.0, respectively. No further increase in the transition temperature was observed with an increasing R ratio. In contrast, previous reports showed that stabilization of the G-quadruplex by ZnTMPyP was significant [27,29]. In accordance with previous reports, the transition temperatures were 54.0 °C and 56.0 °C at R = 0.5 and 1.0, respectively. Considering that the temperature-dependent change in CD reflects the shift in equilibrium from the G-quadruplex to single stranded 5′$G_2T_2G_2TGTG_2T_2G_2$ oligonucleotide,

$$\text{G-quadruplex} \rightleftharpoons \text{Single strand} \tag{3}$$

the equilibrium constant, *K*, can be calculated easily. The logarithm of the temperature-dependent equilibrium constant was plotted as a function of the reciprocal absolute temperature to give the van't Hoff plot (Fig. 5), where *R* is the gas constant.

$$\ln K = -\frac{\Delta H^{\circ}}{R}\left(\frac{1}{T}\right) + \frac{\Delta S^{\circ}}{R} \tag{4}$$

The enthalpy and entropy for transition can be calculated from the slope and *y*-intercept of the plot. At a glance, the unfolding of the G-quadruplex is endothermic with a negative slope in the van't Hoff plot and the entropy change was positive for all cases. In the absence of porphyrin, the enthalpy and entropy were 2.34 ± 0.02 kJ·mol^{-1} and 7.24 ± 0.08 J·mol^{-1}·K^{-1}, respectively. Therefore, the favorable change in entropy causes the unfolding of the G−quadruplex despite its unfavorable change in enthalpy. In the presence of ZnTMPyP, the enthalpy and entropy were 2.26 ± 0.03 kJ·mol^{-1} and 6.88 ± 0.10 J·mol^{-1}·K^{-1}, respectively. Although the difference in enthalpy and entropy in the presence and absence of ZnTMPyP appear to be small, the less favorable entropy change inhibited the unfolding of the G-quadruplex by ZnTMPyP.

3.2. Fluorescence measurements

Fig. 6 and Table 1 show the fluorescence decay profiles of DNA-free porphyrins and those complexed with G-quadruplex. In the absence of G-quadruplex, the decay times of TMPyP were 5.37 ns and 2.18 ns with relative amplitudes of 0.247 and 0.751, respectively (Fig. 6, panel A). These values were in the same range, compared to the reported values [21,46,47]. The short component is normally assigned to TMPyP adsorbed at the surface of the quartz cuvette. Upon binding to G-quadruplex, TMPyP also exhibited two decay times. In the presence of G-quadruplex at R = 1.0, the long decay time increased to 8.76 ns and the short component was 2.06 ns. VOTMPyP also exhibited two decay times in the absence of DNA: 2.24 ns and 6.78 ns with relative

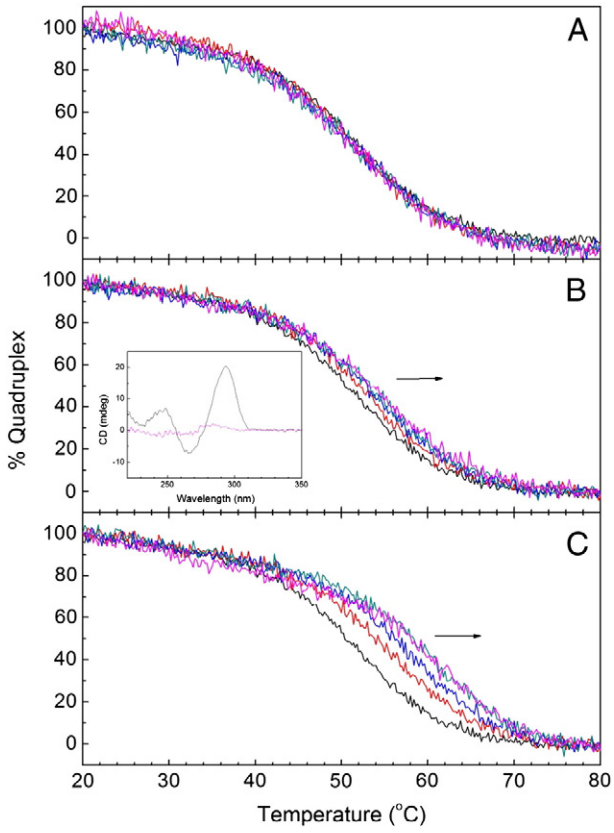

Fig. 4. Thermal denaturation of the G-quadruplex in the presence of TMPyP (panel (A)), VOTMPyP (panel (B)) and ZnTMPyP (panel (C)). The concentration of porphyrins increased to the direction of arrow from 0 to 5 μM with an increment of 1 μM. The temperature-dependent CD intensity of the aptamer $5'G_2T_2G_2TGTG_2T_2G_2$ was recorded at 295 nm. The CD spectrum of the aptamer at 20 °C and 80 °C is inserted in panel (B). [G-quadruplex] = 5 μM. [KCl] = 100 mM.

amplitudes of 0.418 and 0.582, respectively (Fig. 6, panel B). These decay times became 2.06 ns and 9.12 ns upon binding to the G-quadruplex at R = 1.0. In contrast, a single fluorescence decay time of ~1.6 ns was observed in the ZnTMPyP case, and was almost identical in the presence and absence of the G-quadruplex (Fig. 6, panel C).

The intensity of the excitation spectrum increased in the DNA absorption region if the excited energy of DNA bases transfers to G-quadruplex bound porphyrins. When the ratio of the excitation spectrum was plotted with respect to the wavelength in the DNA absorption region, the shape of the resulting plot resembled the DNA absorption spectrum if energy transfer occurred. This resonance-type energy transfer is known as the "contact energy transfer", and is used occasionally as evidence that the ligand and DNA bases are in close proximity [44,45]. Fig. 7 shows the ratio, $Q(\lambda)$ (Eq. (2)), in the DNA absorption region for the porphyrin-G-quadruplex complexes. The rescaled absorption spectrum of the porphyrin-free G-quadruplex is also shown for comparison. For all porphyrins, a large enhancement in the excitation spectrum was observed, and the shape of the $Q(\lambda)$ plot was comparable to that of the G-quadruplex absorption spectrum, suggesting that porphyrins are either in contact with or in the vicinity of the DNA bases. In the TMPyP case, the shape resembles that of the intercalated to double stranded native DNA and poly[d(G–C)$_2$] [45]. On the other hand, enhancement in the fluorescence at short wavelengths was ineffective in the VOTMPyP case.

The fluorescence of all porphyrins in the presence and absence of the G-quadruplex were quenched by I^- ions. Fig. 8 shows the quenching of fluorescence with increasing I^- concentration in the form of the Stern–Volmer plot (Eq. (1)). In the absence of the G-quadruplex, the quenching constant for TMPyP was 180.4 M^{-1}. Those for VOTMPyP and ZnTMPyP were 388.5 M^{-1} and 56.2 M^{-1}, respectively. When associated with the G-quadruplex, the quenching constant decreased significantly. The quenching constant for the TMPyP when bound to the G-quadruplex was 21.9 M^{-1}. In contrast, the I^- quencher was almost inaccessible to TMPyP when it was intercalated between the base-pairs of native calf thymus DNA. The quenching constant for this case was 1.3 M^{-1}, suggesting that the I^- quencher is significantly more accessible to TMPyP when associated with the G-quadruplex compared to that intercalated to double-stranded DNA. The quenching constant for VOTMPyP and ZnTMPyP was 15.5 M^{-1} and 8.7 M^{-1},

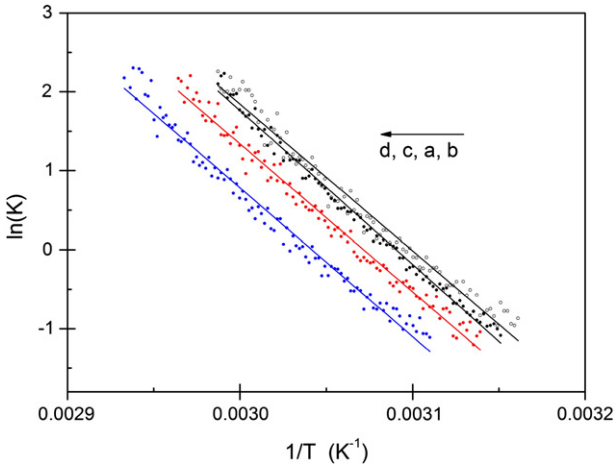

Fig. 5. The van't Hoff plot for denaturation of the G-quadruplex in the absence (a) and presence of TMPyP (b), VOTMPyP (c) and ZnTMPyP (d). The conditions and concentrations are the same as shown in Fig. 4.

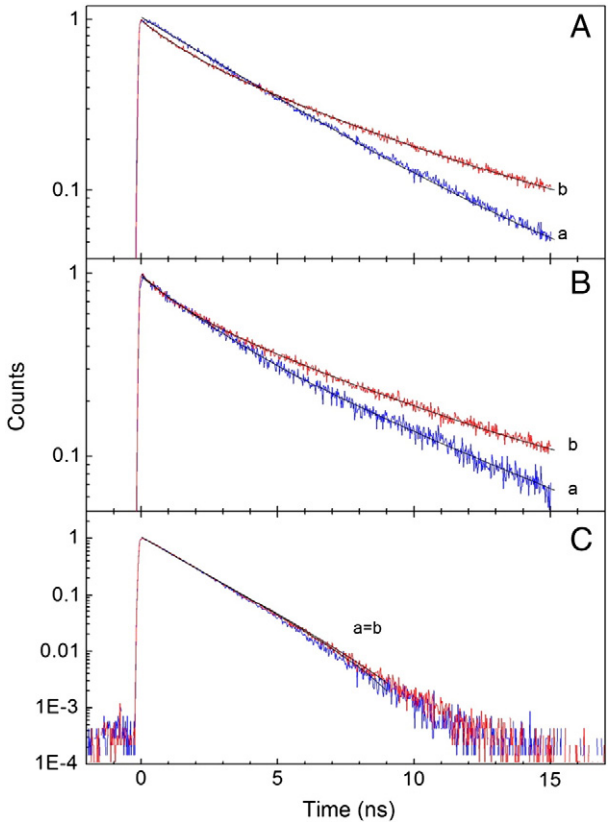

Fig. 6. Fluorescence decay profiles TMPyP (panel (A)), VOTMPyP (panel (B)) and ZnTMPyP (panel (C)) in the absence (curve a) and presence (curve b) of 5 μM G-quadruplex. [TMPyP] = 3 μM. The excitation wavelength was 430 nm and the emission wavelength was 657 nm for TMPyP and VOTMPyP and 630 nm for ZnTMPyP.

Table 1
Fluorescence decay times of the porphyrins in the presence and absence of the G-quadruplex.

	TMPyP	VOTMPyP	ZnTMPyP
DNA-free	$\tau_1 = 2.18$ ns ($a_1 = 0.249$) $\tau_2 = 5.37$ ns ($a_2 = 0.751$)	$\tau_1 = 2.24$ ns ($a_1 = 0.418$) $\tau_2 = 6.78$ ns ($a_2 = 0.582$)	$\tau_1 = 1.58$ ns
G-quadruplex[a]	$\tau_1 = 2.06$ ns ($a_1 = 0.551$) $\tau_2 = 8.76$ ns ($a_2 = 0.449$)	$\tau_1 = 2.06$ ns ($a_1 = 0.457$) $\tau_2 = 9.12$ ns ($a_2 = 0.543$)	$\tau_2 = 1.65$ ns

[a] Decay times in the presence of G-quadruplex were measured at R = 1.0.

respectively, when they are associated with the G-quadruplex. The accessibility of the I^- quencher to G-quadruplex-bound TMPyP decreased by a factor of 8.2 compared to that in the absence of the G-quadruplex. The extent of decrease in accessibility as a result of the association with G-quadruplex was 6.5 for VOTMPyP and was 25.1 for ZnTMPyP. The extent of protection from the I^- quencher by the G-quadruplex was similar for TMPyP and VOTMPyP while it was significantly more efficient for ZnTMPyP.

4. Discussion

Three binding modes for cationic porphyrins to the G-quadruplex have been reported: intercalative binding [20–26,33], end-stacking or stacking at the loops of the quadruplex [18,19,21,27–34,47], and external binding at the grooves of the quadruplex [16,21,35–38]. These binding modes are dependent on a range of factors including the nature of the G-tetraplex, the relative concentration of porphyrins and the nature of the central metal ion of porphyrin.

When associated with a G-quadruplex, the spectral properties of TMPyP are characterized by a red-shift and hypochromism in the absorption spectrum as well as a positive CD band in the Soret region. A large red-shift and hypochromism in the absorption spectrum is generally assigned to the intercalated porphyrin [39]. On the other hand, a comparison of the absorption spectrum of the TMPyP-G-quadruplex adduct with those of the double stranded DNA intercalated ones suggested that the extent of change in the absorption spectrum was not as large. Although the DNA is different, considering that the change in absorption spectrum reflects the extent of π–π stacking and environmental polarity, TMPyP produced less stacking and was more polar when bound to the G-quadruplex than the duplex. Furthermore, TMPyP produced a negative CD when intercalated to double-stranded DNA [39], which is in contrast with the positive CD spectrum observed from the TMPyP-G-quadruplex complex. The relatively large accessibility of the negatively charged external quencher, I^-, also supports the non-intercalative interaction between TMPyP and the G-quadruplex. The quenching efficiency of I^- for TMPyP, which is intercalated between double stranded DNA, was negligible compared to that bound to the G-quadruplex. If TMPyP were intercalated between G-quartet, lower accessibility would be expected considering the size of the intercalation pocket. The intercalation pocket of double-stranded DNA consisted of just two base-pairs, whereas that of the G-quartet is larger, and is expected to provide more protection for TMPyP. The π–π interaction of DNA bases and intercalated ligands helped stabilize the DNA structure. On the other hand, the binding of TMPyP to the G-quadruplex did not increase the thermal stability for the G-quadruplex. These observations are inconsistent with the intercalation binding mode. Accordingly, TMPyP can bind either by stacking at the end, or at the TGT loop, or at

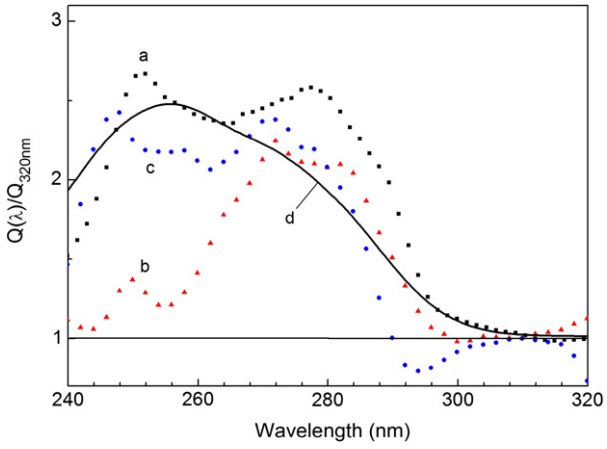

Fig. 7. Contact energy transfer diagram according to Eq. (2) for TMPyP (curve a), VOTMPyP (curve b) and ZnTMPyP (curve c) complexed with G-quadruplex. Rescaled absorption spectrum of G-quadruplex (curve d) is presented for comparison. [G-quadruplex] = 0.5 μM and [porphyrin] = 1.0 μM. The emission wavelengths were the same as those in Fig. 6. The slit widths were 10/10 nm for excitation and emission, respectively.

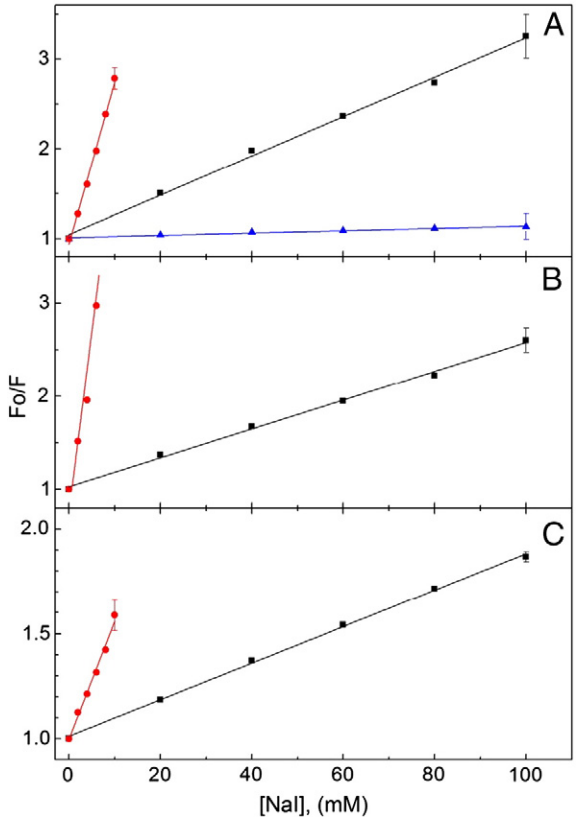

Fig. 8. The fluorescence quenching of TMPyP (panel (A)), VOTMPyP (panel (B)) and ZnTMPyP (panel (C)) in the absence (red circle) and presence of G-quadruplex (black square) by NaI. In panel (A), the quenching of TMPyP that is intercalated to double stranded DNA is presented by blue triangles for comparison. [G-quadruplex] = 0.5 μM and [porphyrin] = 0.3 μM. The $[Na^+]$ concentration was kept constant at 100 μM by adding NaCl. The excitation wavelength was 430 nm and the emission wavelength was 657 nm for TMPyP and VOTMPyP, and 630 nm for ZnTMPyP. The slit widths were 10/10 nm for excitation and emission, respectively. Selective error bars, which represent the standard deviation from five measurements, are shown.

exterior of the G-quadruplex. The invariant absorption and CD spectrum of TMPyP bound to the G-quadruplex at various R ratios indicated that the binding mode is homogeneous and is unaffected by the relative TMPyP population on the G-quadruplex at the R ratio under 1.0. The binding homogeneity is also supported by the quenching property. If there are more than two TMPyP species with different binding modes, i.e. the different accessibility for the I^- quencher, Stern–Volmer plot would not be a straight line.

The changes in the spectral properties of ZnTMPyP upon binding to the G-quadruplex were similar to those in the TMPyP case. ZnTMPyP also produced a red shift and hypochromism in the absorption spectrum, and a positive CD, which was independent of the R ratio, suggesting that the binding mode of ZnTMPyP resembles TMPyP and is homogeneous. On the other hand, the accessibility of the I^- quencher to G-quadruplex-bound ZnTMPyP was 25.1 times lower than that of G-quadruplex-free ZnTMPyP. Protection against the negatively charged I^- quencher by the G-quadruplex is far more effective than TMPyP and VOTMPyP. The decrease in the I^- quencher accessibility by forming the complex with G-quadruplex was 8.2 times and 6.5 times, respectively, for TMPyP and VOTMPyP. This observation suggested that ZnTMPyP binds more tightly to the G-quadruplex. The biexponential fluorescence decay times were observed for TMPyP and VOTMPyP both in the presence and absence of G-quadruplex. The biexponential fluorescence decay of TMPyP in the aqueous solution was attributed to the presence of two types of porphyrin: the long component to free TMPyP in solution and short component to that adsorbed on the surface of quartz cuvette [46]. The long decay component of TMPyP and VOTMPyP became longer upon binding to the G-quadruplex. Contrarily, ZnTMPyP produced a single exponential curve in the fluorescence decay both in the presence and absence of the G-quadruplex. The decay times were almost identical. Although the fluorescence decay profiles cannot be fully elucidated at this stage, it is clear that ZnTMPyP is different from TMPyP and VOTMPyP when bound to the G-quadruplex. Although the fluorescence properties of VOTMPyP including the elongation of decay time and extent of decrease in the accessibility of I^- quencher upon association with G-quadruplex are similar to TMPyP, the π–π interaction between VOTMPyP and the G-quartet appears to be weakest because no red shift and small hypochromism was observed for the G-quadruplex-bound VOTMPyP.

Stabilization of the G-quadruplex by ZnTMPyP has been reported [27,29]. In accordance with previous reports, ZnTMPyP was the most effective in stabilizing the G-quadruplex among the porphyrins tested. Although it was less effective, VOTMPyP also stabilized the G-quadruplex while TMPyP slightly destabilized the G-quadruplex. Stabilization of the G-quadruplex or resistance against thermal denaturation by the metallo-porphyrins appears to be due mainly to the entropic effect because the slope in the van't Hoff plot was similar in the presence and absence of porphyrins. Therefore, the role of a π–π interaction between porphyrin and G-quartet might not be the main factor in stabilizing the G-quadruplex because destacking of the π–π interaction requires the energy related to a change in both entropy and enthalpy. Furthermore, stabilization by VOTMPyP, for which there is no evidence of stacking, is also effective but its efficiency is lower than that of ZnTMPyP. Although the structure of ZnTMPyP is generally planar and is coordinated with the four N atoms of TMPyP [48], *penta*-coordination in an aqueous environment with its fifth ligand being a water molecule was also reported [49]. Based on the possibility of the fifth ligation, the stabilization of the G-quadruplex by ZnTMPyP might be caused by coordination of the central Zn ion with any of the G-quadruplex components. From this suggestion, stabilization of the G-quadruplex by VOTMPyP for which there is no evidence of π–π stacking can be explained. A water molecule can bind to the central vanadium at the opposite site of the oxygen molecule coordinated site [50]. Therefore, similarly to the ZnTMPyP case, it is possible that one of the G-quartet components coordinated with the central vanadium ion, thereby stabilizing the structure of the G-quadruplex.

5. Conclusion

TMPyP, VOTMPyP and ZnTMPyP do not intercalate and bind at the exterior of the G-quadruplex formed from an aptamer, $5'G_2T_2G_2TGTG_2T_2G_2$. ZnTMPyP and VOTMPyP effectively stabilized the G-quadruplex, whereas TMPyP only slightly destabilizes it. The efficiency of stabilization was the highest for ZnTMPyP.

Acknowledgment

This study was supported by the Korea Research Foundation (Grant no. 2012-008875, conferred to S. K. Kim) and by the KRISS Program (Grant no. 13011047).

References

[1] J.L. Huppert, Structure, location and interaction of G-quadruplexes, FEBS J. 277 (2010) 3452–3458.
[2] H.J. Lipps, D. Rhodes, G-quadruplex Structures: in vivo evidence and function, Trends Cell Biol. 19 (2009) 414–422.
[3] J.L. Huppert, Hunting G-quadruplexes, Biochimie 90 (2008) 1140–1148.
[4] S. Burge, G.N. Parkinson, P. Hazel, A.K. Todd, S. Neidle, Quadruplex DNA: sequence, topology and structure, Nucleic Acids Res. 34 (2006) 5402–5415.
[5] N. Maizels, Dynamic roles for G4 DNA in the biology of eukaryotic cells, Nat. Struct. Mol. Biol. 13 (2006) 1055–1059.
[6] Y. Wu, R.M. Brosh Jr., G-quadruplex nucleic acids and human disease, FEBS J. 277 (2010) 3470–3488.
[7] S.N. Georgiades, N.H. Abd Karim, K. Suntharalingam, Interaction of metal complexes with Q-quadruplex, Angew. Chem. Int. Ed. 49 (2010) 4020–4034.
[8] J.E. Reed, A. Arola-Arnal, S. Neidle, V. Ramón, Stabilization of G-quadruplex DNA and inhibition of telomerase activity by square-planar nickel(II) complexes, J. Am. Chem. Soc. 128 (2006) 5992–5993.
[9] A. Arola-Arnal, J. Benet-Buchholz, S. Neidle, R. Vilar, Effects of metal coordination geometry on stabilization of human telomeric quadruplex DNA by square-planar and square-pyramidal metal complexes, Inorg. Chem. 47 (2008) 11910–11919.
[10] H. Bertrand, D. Monchaud, A. De Cian, R. Guillot, J.-L. Mergny, M.-P. Teulade-Fichou, The importance of metal geometry in the recognition of G-quadruplex-DNA by metal-terpyridine complexes, Org. Biomol. Chem. 5 (2007) 2555–2559.
[11] K. Suntharalingam, A.J.P. White, R. Vilar, synthesis, structural characterization, and quadruplex DNA binding studies of platinum(II)-terpyridine complexes, Inorg. Chem. 48 (2009) 9427–9435.
[12] W.-J. Mei, X.-Y. Wei, Y.-J. Liu, B. Wang, Studies on the interactions of a novel ruthenium(II) complex with G-quadruplex DNA, Transit. Met. Chem. 33 (2008) 907–910.
[13] J. Talib, C. Green, K.J. Davis, T. Urathamakul, J.L. Beck, J.R. Aldrich-Wright, S.F. Ralph, A comparison of the binding of metal complexes to duplex and quadruplex DNA, Dalton Trans. (2008) 1018–1026.
[14] S. Shi, J. Liu, T. Yao, X. Geng, L. Jiang, Q. Yang, L. Cheng, L. Ji, Promoting the formation and stabilization of G-quadruplex by dinuclear Ru^{II} complex $Ru_2(obip)L_4$, Inorg. Chem. 47 (2008) 2910–2912.
[15] C. Rajput, R. Rutkaite, L. Swanson, I. Haq, J.A. Thomas, Dinuclear monointercalating Ru^{II} complexes that display high affinity binding to duplex and quadruplex DNA, Chem. Eur. J. 12 (2006) 4611–4619.
[16] I.M. Dixon, F. Lopez, A.M. Tejera, J.-P. Estève, M.A. Blasco, G. Pratviel, B. Meunier, A G-quadruplex ligand with 10000-fold selectivity over duplex DNA, J. Am. Chem. Soc. 129 (2007) 1502–1503.
[17] D.-F. Shi, R.T. Wheelhouse, D. Sun, L.H. Hurley, Quadruplex-interactive agents as telomerase inhibitors: synthesis of porphyrins and structure-activity relationship for the inhibition of telomerase, J. Med. Chem. 44 (2001) 4509–4523.
[18] R.T. Wheelhouse, D. Sun, H. Han, F.X. Han, L.H. Hurley, Cationic porphyrins as telomerase inhibitors: the interaction of tetra-(N-methyl-4-pyridyl)porphine with quadruplex DNA, J. Am. Chem. Soc. 120 (1998) 3261–3262.
[19] E. Izbicka, R.T. Wheelhouse, E. Raymound, K.K. Davidson, R.A. Lawrence, D. Sun, B.E. Windle, L.H. Hurley, D.D. Von Hoff, Effects of cationic porphyrins as G-quadruplex interactive agents in human tumor cells, Cancer Res. 59 (1999) 639–644.
[20] M. Cavallari, A. Garbesi, R.D. Felice, Porphyrin intercalation in G-4-DNA quadruplexes by molecular dynamic simulations, J. Phys. Chem. B 113 (2009) 13152–13160.
[21] C. Wei, G. Jia, J. Zhou, G. Han, C. Li, Evidence for the binding mode of porphyrins to G-quadruplex DNA, Phys. Chem. Chem. Phys. 11 (2009) 4025–4032.
[22] M. Del Toro, R. Gargallo, R. Eritja, J. Jaumot, Study of the interaction between the G-quadruplex-forming thrombin-binding aptamer and the porphyrin 5,10,15,20-tetrakis-(*N*-methyl-4-pyridyl)-21,23H-porphyrin tetratosylate, Anal. Biochem. 379 (2008) 8–15.
[23] I. Lubitz, N. Borovok, A. Kotlyar, Interaction of monomolecular G4-DNA nanowires with TMPyP: evidence for intercalation, Biochemistry 46 (2007) 12925–12929.
[24] C. Wei, G. Jia, J. Yuan, Z. Feng, C. Li, A spectroscopic study on the interactions of porphyrin with G-quadruplex DNAs, Biochemistry 45 (2006) 6681–6691.
[25] I. Haq, J.O. Trent, B.Z. Chowdhry, T.C. Jenkins, Intercalative G-tetraplex stabilization of teomeric DNA by a cationic porphyrin, J. Am. Chem. Soc. 121 (1999) 1768–1779.

[26] N.V. Anantha, M. Azam, R.D. Sheardy, Porphyrin binding to quadruplexed T4G4, Biochemistry 37 (1998) 2709–2714.
[27] A.J. Bhattacharjee, K. Ahluwalia, S. Taylor, O. Jin, J.M. Nicoludis, R. Buscaglia, J.B. Chaires, D.J.P. Kornfilt, D.G.S. Marquardt, L.A. Yatsunyk, Induction of G-quadruplex DNA structure by Zn(II) 5,10,15,20-tetrakis(*N*-methyl-4-pyridyl)porphyrin, Biochimie 93 (2011) 1297–1309.
[28] C. Wei, J. Wang, M. Zhang, Spectroscopic study on the binding of porphyrins to $(G_4T_4G_4)_4$ parallel G-quadruplex, Biophys. Chem. 148 (2010) 51–55.
[29] J. Pan, S. Zhang, Interaction between cationic zinc porphyrin and lead ion induced telomeric guanine quadruplexes: evidence for end-stacking, J. Biol. Inorg. Chem. 14 (2009) 401–407.
[30] G. Jia, Z. Feng, C. Wei, J. Zhou, X. Wang, C. Li, Dunamic insight into the interaction between porphyrin and G-quadruplex DNAs: time-resolved fluorescence anisotropy study, J. Phys. Chem. B 113 (2009) 16237–16245.
[31] G.N. Parkinson, R. Ghosh, S. Neidle, Structural basis for binding of porphyrin to human telomeres, Biochemistry 46 (2007) 2390–2397.
[32] S.E. Evans, M.A. Mendez, K.B. Turner, L.R. Keating, R.T. Grimes, S. Melchoir, V.A. Szalai, End-stacking of copper cationic porphyrins on parallel-stranded guanine quadruplexes, J. Biol. Inorg. Chem. 12 (2007) 1235–1249.
[33] L.R. Keating, V.A. Szalai, Parallel-stranded quadruplex interactions with a copper cationic porphyrin, Biochemistry 43 (2004) 15891–15900.
[34] H. Han, D.R. Langley, A. Rangan, L.H. Hurley, Selective interactions of cationic porphyrins with G-quadruplex structures, J. Am. Chem. Soc. 123 (2001) 8902–8913.
[35] A. Arora, S. Maiti, Effect of loop orientation on quadruplex-TMPyP4 interaction, J. Phys. Chem. B 112 (2008) 8151–8159.
[36] K. Halder, S. Chowdhury, Quadruplex-coupled kinetic distinguishes ligand binding between G4 DNA motifs, Biochemistry 46 (2007) 14762–14770.
[37] J. Seenisamy, S. Bashyam, V. Gokhale, H. Vankayalapati, D. Sun, A. Siddiqui-Jain, N. Streiner, K. Shin-Ya, E. White, W.D. Wilson, L.H. Hueley, Design and synthesis of an expanded porphyrin that has selectivity for the c-MYC G-quadruplex structure, J. Am. Chem. Soc. 127 (2005) 2944–2959.
[38] T. Yamashita, T. Uno, Y. Ishikawa, Stabilization of guanine DNA by the binding of porphyrins with cationic side arms, Bioorg. Med. Chem. 13 (2005) 2423–2430.
[39] L. Gong, I. Bae, S.K. Kim, Effect of axial ligand on the binding mode of M-*meso*-tetrakis(*N*-methylpyridium-4yl)porphyrin to DNA probed by circular and linear dichroism spectroscopies, J. Phys. Chem. B 116 (2012) 12510–12521.
[40] Y.R. Kim, L. Gong, J.J. Park, Y.J. Jang, J. Kim, S.K. Kim, Systematic investigation on the central metal ion dependent binding geometry of M-*meso*-tetrakis(*N*-methylpyridium-4yl)porphyrin to DNA and their efficiency as an acceptor in DNA-mediated energy transfer, J. Phys. Chem. B 116 (2012) 2330–2337.
[41] K.Y. Wang, S. McCurdy, R.G. Shea, S. Swaminathan, P.H. Bolton, A DNA aptamer which binds to and inhibits thrombin exhibits a new structural motif for DNA, Biochemistry 32 (1993) 1899–1904.
[42] H.S. Cho, N.W. Song, Y.H. Kim, S.C. Jeoung, S. Hahn, D. Kim, Ultrafast energy relaxation dynamics of directly linked porphyrin arrays, J. Phys. Chem. A 104 (2000) 3287–3298.
[43] J.R. Lakowicz, Principles of Fluorescence Spectroscopy, 3rd ed. Springer Sci., N. Y., 2006. 277–318.
[44] J.B. Le Pecq, C. Paoletti, J. Mol. Biol. 29 (1967) 87–106.
[45] K.-M. Hyun, S.D. Choi, S. Lee, S.K. Kim, Can energy transfer be an indicator for DNA intercalation? Biochim. Biophys. Acta 1334 (1997) 312–326.
[46] F.J. Vergeldt, R.B. M. Koehorst, A. van Hoek, T.J. Schaafsma, Intramolecular interactions in the ground and excited state of tetrakis(*N*-methyl)pyridyl)porphyrins, J. Phys. Chem. 99 (1995) 4397–4405.
[47] C. Wei, L. Wang, G. Jia, J. Zhou, G. Han, C. Li, The binding mode of porphyrins with cation side arms to $(TG_4T)4$ G-quadruplex: spectroscopic evidence, Biophys. Chem. 143 (2009) 79–84.
[48] R. Slota, M.A. Broda, G. Dyrda, K. Ejsmont, G. Mele, Structural and molecular characterization of *meso*-substituted zinc porphyrins: a DFT supported study, Molecules 16 (2011) 9957–9971.
[49] A.J. Golder, D.C. Povey, J. Silver, Q.A.A. Jassim, Structure of aqua(tetraphenylporphyrinato) zinc(II): a redetermination, Acta Crystallogr. C46 (1990) 1210–1212.
[50] D.W. Cho, D.H. Jeong, J.-H. Ko, S.K. Kim, M. Yoon, Raman spectroscopic studies on interactions of water soluble cationic oxovanadyl(IV) *meso*-tetrakis(1-methylpyridium-4-yl) porphyrin with nucleic acids, J. Photochem. Photobiol. A Chem. 174 (2005) 207–213.